1 Constraint on net primary productivity of the global ocean by Argo oxygen measurements

Kenneth S. Johnson¹ and Mariana B. Bif¹

2 ¹Monterey Bay Aquarium Research Institute, Moss Landing, CA, USA

3

The biological transformation of dissolved inorganic carbon to organic carbon during 4 5 photosynthesis in the ocean, marine primary production, is a fundamental driver of 6 biogeochemical cycling, ocean health and the earth's climate system. The organic matter 7 created supports oceanic food webs including fisheries and is an essential control on 8 atmospheric carbon dioxide levels. Marine primary productivity is sensitive to changes due to 9 climate forcing but observing the response at the global scale remains a significant challenge. 10 Sparsely distributed productivity measurements are made using samples collected and analyzed on research vessels. However, there are never enough ships and scientists to enable 11 12 direct observations at the global scale with seasonal to annual resolution. Today, global ocean productivity is estimated using remote sensing ocean colour observations or general 13 14 circulation models with coupled biological models that are calibrated with the sparse 15 shipboard measurements. Here we demonstrate the measurement of gross oxygen 16 production by photosynthesis using the diel cycle of oxygen concentration detected with the 17 array of Biogeochemical-Argo (BGC-Argo) profiling floats. The global ocean net primary

productivity computed from this data is 53 Pg C y⁻¹, which will be a significant constraint on

satellite and general circulation model (GCM)-based estimates of the ocean productivity.

19 20 21

22

23

2425

26

27

28

29

30

18

Global ocean productivity is estimated to be near half of the Earth's total productivity¹ and it represents the production of autotrophic biomass that is readily available for the remaining food web^{2, 3, 4}. Uptake of inorganic carbon and sinking of the particulate organics sequesters atmospheric carbon into the ocean interior, a process known as the biological carbon pump⁵. This process reduces the present atmospheric CO₂ by 200 ppm relative to a world with a modeled, abiotic ocean⁶. Measuring metabolic rates via daily photosynthetic generation of oxygen (gross oxygen production, GOP), total carbon dioxide reduction (gross primary production, GPP) and net primary production (NPP which equals GPP minus autotroph respiration to sustain self-metabolism) have been valuable tools to assess the marine ecosystem status and productivity⁴. In a changing ocean, primary productivity is observed to be variable spatially and seasonally^{7, 8, 9}.

313233

34

35

The earliest measurements of primary productivity in the ocean were based on the Light Bottle/Dark Bottle (LBDB) methodology, resulting in GOP rates¹⁰. Poor sensitivity and bottle artifacts led to replacement of the LBDB method by ¹⁴C-bicarbonate labeled incubations¹¹ as

the most generally utilized method. It is interpreted to yield net primary productivity estimates^{2, 12, 13}, although method artifacts may still occur^{13, 14}. Early assessments of global primary productivity were based on extrapolation of ¹⁴C-labeled NPP measurements to the entire ocean^{10, 15}. More recently, methods based on the fractionation of the three isotopes of oxygen have been used to determine GOP rates directly from samples without the need for incubation^{16, 17}. However, there are never enough of any of these measurements to enable the extrapolation to a global extent with seasonal to annual resolution.

With the advent of satellite based observations of chlorophyll near the sea surface, a variety of methods to estimate the ocean's biological productivity were developed ^{18, 19}. These estimates were based on empirical models of primary production ^{20, 21} that have been tuned to a limited set of ¹⁴C-uptake NPP observations (Figure 1a) and driven by the satellite fields of chlorophyll and carbon. More recently, global estimates of ocean primary productivity have been generated using general circulation models (GCM) with embedded biogeochemical models that assimilate ocean color data ^{22, 23}. These satellite and GCM methods generate net primary productivity in the range of 30 to 60 Pg C y⁻¹ for the global ocean ^{18, 22, 24}. None of these values are direct observations of ocean productivity, however. They are estimates derived from models with documented limitations ^{18, 19, 23}. For instance, these models have difficulty reproducing observations at ocean time series stations ²⁵ and they may be affected by changing phytoplankton physiology ²⁶.

In an approach derived from the original LBDB method, autonomous platforms equipped with oxygen sensors are now capable of measuring the diel cycle of oxygen production and respiration directly in the open ocean without enclosing samples^{27, 28}. This has enabled direct observations of GOP and community respiration (CR, respiration at all trophic levels) in oligotrophic waters^{29, 30, 31}. These approaches require multiple observations over the course of each day from a single autonomous platform and they are difficult to replicate to the global scale.

Observing diel oxygen cycles

Here we use the profiling floats of the Biogeochemical-Argo (BGC-Argo) array³² to detect the diel cycle of oxygen (GOP) and compute net primary productivity at the global scale (Figure 1b). BGC-Argo floats are free drifting platforms equipped with biological and chemical sensors, including oxygen, that profile from ~2000 m depth to surface. Observations made on the ascent are transmitted via satellite to Argo Data Assembly Centers, where results are made available without restriction within 24 hours. Each float has sufficient energy to make about 200 vertical profiles, typically at ~5 to ~10 day intervals over float lifetimes that reach 4 to 6 years. The low profiling frequency would seem to be incompatible with the need for multiple measurements during one day to detect a diel oxygen cycle. However, the diel cycle of oxygen is a signal that is phase locked to the solar cycle. This signal is present in euphotic zone oxygen concentrations throughout the ocean and it can be resolved using the methods shown here. Exact calibration of the oxygen sensors in the array is not required.

Detecting diel cycles from the Argo array has been demonstrated previously. Gille³³ found that the diel cycle of temperature in the upper ocean is observable when the array is used as a collective set of sensors. Gille introduced one additional protocol to improve the statistical performance of such calculations. The analysis used the anomaly of the profiling float temperatures relative to a reference value rather than analyzing the float temperature directly. The reference for temperature observations was the temperature measured at local noon (or midnight) near each float profile by orbiting satellites. The use of temperature anomalies reduces the variability in the data. In the case of profiling float oxygen, we use the anomaly of oxygen concentration relative to atmospheric saturation (saturation anomaly) in each sample for our GOP calculations. The oxygen concentrations in the upper 10 m and the saturation anomaly for all Argo data in the upper 10 m are shown in Extended Data Figure S1.

To illustrate the phase locked oxygen signal, the oxygen concentration anomaly (oxygen – atmospheric saturation concentration in the same water) data in the upper 20 m from 60°N to 10°N are shown versus the local hour of day when the samples were obtained (Figure 2a). Although the individual profile data are scattered, a diel signal is clear when the mean oxygen anomaly value in each hour of the pseudo-daily cycle is computed (Figure 2b). This plot was made with adjusted oxygen data from floats in the Argo Global Data Assembly Center that have sampled all hours of the day evenly (see Methods) from 2010 through 2020. 14,294 profiles of 50,736 oxygen profiles from this region have the required float timing with all hours of the day sampled at nearly even occurrences. The remaining profiles could not be used to assess the diel cycle because those floats sampled at one or a few fixed hours of the day. Any calibration offsets in floats that sample at fixed times will corrupt the diel signal by biasing only the few sampled hours of the day.

A GOP annual rate of 2.2 ± 0.3 (1 Std. Error, N=14,294) mmol O_2 m⁻³ d⁻¹ was obtained from the data (Figure 2b). The procedure used to fit the GOP rate (Methods) is based on the approach outlined by Barone et al.²⁹. Standard error limits were calculated using bootstrapping²⁹. The typical least squares fit error gave similar results. A seasonal cycle in GOP is resolved with a spring maximum (Figure 2c). The annually averaged and vertically integrated GOP rate to 50 m depth (Figure 2d) is 70 ± 12 mmol O_2 m⁻² d⁻¹. This analysis was limited to the northern hemisphere to preserve the seasonal signal. The entire global data set can be used (Extended Data Figure S2) to obtain a rate of 2.1 ± 0.4 mmol O_2 m⁻³ d⁻¹ in the upper 20 m. This rate is a somewhat spatially biased (Figure 1b) estimate of the global mean GOP rate. The calculations we applied assume negligible effects on computed GOP from the diel temperature cycle, from gas exchange, and a presumption that GOP equals CR. The effects of these assumptions are explored in the Methods. The only limitation on resolving the diel signal and obtaining a GOP rate by this approach is having sufficient profiles in the geographic and temporal region that sample all hours of the day. These limits are considered below.

Productivity near Hawaii and Bermuda

Floats are not anchored and the configuration of the array for each hour will be different.

There must be sufficient observations in each particular region to provide an adequate

representation of the oxygen anomaly value at every hour of the day. The adequacy of this assumption was tested by computing GOP with profiles near the Hawaii Ocean Time-series (HOT) station and the Bermuda Atlantic Time-series Station (BATS). GOP determined from float profiles near the two stations (Figure 1b) were compared with productivity determined from ship-based sampling. The pseudo-daily cycle near HOT (Figure 3a) was determined from 1791 vertical profiles collected from 2010 through 2020 within a geographic box (21 to 25°N, 165 to 150°W; Figure 1b) that encompasses HOT. The hourly binned data (Figure 3b) show the daily oxygen cycle with a 0.8 µmol kg⁻¹ daily amplitude in the upper 20 m. A statistically significant (p<0.0005) GOP of 1.5 \pm 0.3 (1 Std. Error) mmol O₂ m⁻³ d⁻¹ in the upper 20 m was obtained²⁹ from the fit to the data in Figure 3a. This represents the annual mean GOP over the past 11 years. In comparison, Barone et al.²⁹ have tabulated 11 reports of GOP in the mixed layer at HOT with a mean of 1.3±0.5 (1 SD) mmol O₂ m⁻³ d⁻¹. The GOP integrated to 100 m, near the 1% light level, was 103±18 mmol O₂ m⁻² d⁻¹ (Figure 2c). The mean integral observed by Juranek and Quay³⁴ on four cruises near HOT in 2002 and 2003 was 111±51 (1 SD) mmol O₂ m⁻² d⁻¹ while Quay et al.³⁵ found 103±43 mmol O₂ m⁻² d⁻¹ on multiple cruises from 2006 to 2008 using the triple oxygen isotope method.

The annual cycle of GOP in the upper 20 m near HOT was computed from the float data with two month resolution (Figure 3c). This is the highest temporal frequency that can be resolved in the float data with ~2000 total profiles (see below). The monthly mean NPP rates in the upper 20 m that were measured by ¹⁴C-labeled incubations in the HOT program are shown for comparison. The ratio of GOP/NPP was found to be consistently near 2.7 during the JGOFS program¹² and between 2 to 3 near the surface at HOT³⁵. The NPP rates measured at HOT (Figure 3c, d) are plotted on a scale that is a factor of 2.5 smaller than the GOP scale. Both sets of data show a relatively flat seasonal cycle with GOP about 2.5 times greater than the NPP near the surface. The weak seasonal signal is consistent with GOP observations at HOT³⁶. The vertical profile of GOP at 10 m intervals is shown in Figure 3d. GOP decreased with depth in parallel with the observed decrease in NPP and was approximately 2.5 times greater than the NPP values throughout the profile. The larger error limits on GOP at depth preclude detection

of the change in GOP/NPP observed by Quay et al.³⁵ at HOT.

Figures 3e-f show similar results for float profiles in the geographic box (28 to 38°N, 75 to 55°W; Figure 1b) that encompasses BATS. There are 741 profiles that are suitable for analysis. The error bars at each hour (Figure 3f) are larger than near HOT due to fewer profiles and a larger temperature range that creates greater spread in the oxygen anomaly data. A statistically significant (p<0.014) diel signal with a GOP rate of 2.3±0.9 mmol O_2 m⁻³ d⁻¹ in the upper 20 m was obtained for all data in the 2010 through 2020 period. The GOP rate vertically integrated to 80 m at BATS (Figure 3h) is 148±44 mmol O_2 m⁻² d⁻¹. In comparison, Luz and Barakan³⁷ found a mean GOP value of 70±24 mmol O_2 m⁻² d⁻¹. The annual cycle derived from float data (Fig. 3g) was computed at quarterly intervals because of the smaller number of profiles near BATS. In contrast to HOT, the GOP values decreased appreciably over the course of the year. This decrease was mirrored in the measured NPP data. The high productivity in late winter results from entrainment of nitrate into the mixed layer³⁸. The GOP/NPP ratios at BATS during winter and late fall are consistent with the canonical value of 2.7 reported for JGOFS samples¹². During

summer, the ratios of GOP/NPP in Figure 3g were higher than 2.7, with values up to 5. Higher ratios of GOP/NPP at BATS during spring and summer, in the range of 3 to 7, have been noted previously^{16, 17}. High GOP/NPP may result from the production of Gel-Like Organic Matter (GLOM) during NPP incubations that is not trapped on filters³⁹. GLOM would lead to an underestimate of primary productivity and elevated GOP/NPP ratios.

173 174 Glob

Global ocean productivity

175176

177178

179

180

181

182

183

184

168

169

170

171

172

The diel cycles of oxygen can be used to compute global ocean GOP and NPP rates between 60°N to 60°S in the deep waters (>2000 m) where floats operate. To minimize biases due to clusters of profiles in various regions (Figure 1b), we have computed zonal mean GOP by 10° bands of latitude from 60°N to 60°S (Table 1). This is a balance between spatial resolution and having sufficient float profiles to minimize errors in GOP. We have also combined observations from all years to minimize spatial biases. Interannual changes have not been computed as they reflect significant geographic change in the float array over time. We assume a value of 2.7 for the GOP/NPP ratio 12, 17 to enable NPP calculations that illustrate the consistency of the GOP determinations on a broad scale. However, the GOP/NPP ratio can vary at times from a value of 2.7, as noted above, in a manner that is not yet well understood.

185 186 187

188 189

190

191

192

193

194

195

196

197

198 199

200

201202

203

204

205

206

207

A GOP rate of 10.4±1.6 Pmol O₂ y⁻¹, and a net primary productivity of 46±7 Pg C y⁻¹ were obtained by summing the values in each latitude band (Table 1). The areas in Table 1 include water shallower than 2000 m, effectively extrapolating low open ocean rates to the entire zone. NPP errors reflect only the uncertainty in the GOP rates and not the GOP/NPP ratio. The total float GOP was adjusted to a global extent as described in the Methods. This yields 11.9±1.9 Pmol O₂ y⁻¹, which is consistent with global GOP (9.5 to 12.6 Pmol O₂ y⁻¹) determined from a neural network fitted to a global set of LBDB and triple oxygen isotope measurements⁴⁰. The NPP values derived from the diel oxygen cycles are compared to values derived from satellite ocean colour data using the VGPM²¹, CBPM²⁴, and CAFE⁴¹ productivity models in Table 1 and Extended Data Figure S3. The satellite observations were limited to latitudes from 50°N to 50°S because monthly climatologies poleward have missing data during many months. The VGPM total is lower than the observed float value while the CBPM and CAFE models are similar (Table 1). There are apparent differences in the distribution of primary productivity with latitude (Table 1; Extended Data Figure S3). The float data imply a much greater contrast between NPP in equatorial regions versus the sub-tropics (Extended Data Figure S3a). The ocean colour NPP models are in reasonable agreement with the float data at latitudes poleward of 30°. If the profiling float NPP result in Table 1 is adjusted to a global extent, as for GOP (Methods), then a global NPP of 53±7 Pg C y⁻¹ is obtained. This is consistent with the CBPM and CAFE global totals (52 Pg C y⁻¹) and the mean, global NPP (51 Pg C y⁻¹) found in a comparison of 24 NPP algorithms¹⁸. While significant areas (e.g., 0 to 20° S) of the ocean now have insufficient data for analysis of diel oxygen cycles, the coverage is greater than that of the primary productivity stations used to constrain productivity models (Figure 1).

208209210

211

The spatial resolution of the GOP measurements is limited by the number of operating floats and the number of profiles needed to resolve the diel cycle. Twenty to fifty profiles in each hour

212 of the pseudo-day are required to clearly resolve diel changes with variability similar to that in 213 Figure 2a and 3a. The smaller number of profiles pertain to tropics with low oxygen variability 214 and larger numbers to high latitudes. With 36 profiles per year from a float at the standard 10 215 day cycle time, accurate GOP determination of annual cycles will require 12 (tropics) to 30 (high latitude) float years of data. The Biogeochemical-Argo Implementation Plan⁴² calls for a global 216 array of 1000 floats, versus 377 floats now operating, although fewer than one half are 217 operating with the required cycle timing. The low number of floats available in any one year 218 was overcome in this work by binning 11 calendar years of data. In the future, the size of the 219 220 BGC-Argo fleet will increase as the Global Ocean Biogeochemistry Array (GO-BGC) project will produce an array of 500 floats that are evenly distributed and which will operate with the 221 required timing properties needed to detect diel oxygen cycles. The GO-BGC array will produce 222 223 a much more evenly distributed array and diminish spatial biases due to gaps in the profiling 224 float array (Figure 1b). However, even at a maximum array size of 1000 floats and with all floats 225 operating with appropriate cycle timing, the GOP or NPP rates would resolve annual cycles in 226 only about 50 regions in the ocean. Thus, this method cannot approach the resolution obtained by satellites. Assimilating the observed diel cycles at low resolution into high resolution GCMs 227 along with satellite chlorophyll fields will mitigate this issue and contribute to a more accurate 228 representation of the ocean productivity⁴³. 229

230

231

Data availability

- The profiling float data used in this study was obtained in December 2020 by downloading all
- 233 Argo Sprof files directly from the Argo Global Data Assembly Center
- 234 (ftp://usgodae.org/pub/outgoing/argo or ftp://ftp.ifremer.fr/ifremer/argo). The corresponding
- 235 monthly snapshot (December 2020) of the Argo database, which contains these Sprof files in
- addition to floats that do not have biogeochemical sensors, is
- 237 https://doi.org/10.17882/42182#79118. The Sprof files for floats with adjusted oxygen
- concentrations were then merged into netCDF files for the Northern and Southern
- 239 Hemispheres and used for the analyses reported here. These files are available at
- 240 https://doi.org/10.5281/zenodo.4989023. Monthly satellite data were down loaded from
- 241 http://www.science.oregonstate.edu/ocean.productivity/.

242

243

Code Availability

- Analyses were performed in Matlab. Code used in this analysis is available at
- 245 https://doi.org/10.5281/zenodo.4989023.

¹ Field, C., Behrenfeld, M., Randerson, J. & Falkowski, P. Primary production of the biosphere: integrating terrestrial and oceanic components. *Science* **281**, 237–240 (1998).

- ³ Falkowski, P. G. The role of phytoplankton photosynthesis in global biogeochemical cycles. *Photosynth. Res.* **39**, 235–258 (1994).
- ⁴ Chavez, F. P., Messié, M. & Pennington, J. T. Marine primary production in relation to climate variability and change. *Ann. Rev. Mar. Sci.* **3**, 227–260 (2011).
- ⁵ Ducklow, H. W., Steinberg, D. K. & Buesseler, K. O. Upper ocean carbon export and the biological pump. *Oceanography* **14**, 50-58 (2001).
- ⁶ Watson, A. J. & Orr, J. C. Carbon Dioxide Fluxes in the Global Ocean. In: *Ocean Biogeochemistry* (ed Fasham M. J. R.) 123-143 (Springer, New York, 2003).
- ⁷ Steinacher, M. et al. Projected 21st century decrease in marine productivity: a multi-model analysis. *Biogeosci.* **7**, 979-1005 (2010).
- ⁸ Bryndum-Buchholz, A. et al. Twenty-first-century climate change impacts on marine animal biomass and ecosystem structure across ocean basins. *Global Change Biol.* **25**, 459-472 (2019).
- ⁹ Kavanaugh, M. T., Church, M. J., Davis, C. O., Karl, D. M., Letelier, R. M. & Doney, S. C. ALOHA from the edge: reconciling three decades of in situ eulerian observations and geographic variability in the North Pacific Subtropical Gyre. *Front. Mar. Sci.* **5**, 130 (2018).
- ¹⁰ Barber, R. T. & Hilting, A. K. History of the study of plankton productivity. In *Phytoplankton Productivity: Carbon Assimilation in Marine and Freshwater Ecosystems*, (eds Williams, P. J. L., Thomas, D. N. & Reynolds, C. S.) 16-43 (Blackwell, Malden, Mass., 2002).
- ¹¹Steeman Nielsen, E. The use of radioactive carbon (C^{14}) for measuring organic production in the sea. *ICES J. Mar. Sci.* **18**, 117-140 (1952).
- ¹² Marra, J. Approaches to the measurement of plankton production. In *Phytoplankton Productivity: Carbon Assimilation in Marine and Freshwater Ecosystems*, (eds Williams, P. J. L., Thomas, D. N. & Reynolds, C. S.) 78–108 (Blackwell, Malden, Mass., 2002).
- ¹³ Marra, J. Net and gross productivity: weighing in with ¹⁴C. *Aquatic Micro. Ecol.*, **56**, 123-131 (2009).
- ¹⁴ Fitzwater, S. E., Knauer, G. A. & Martin, J. H. Metal contamination and its effect on primary production measurements 1. *Limnol. Oceanogr.* **27**,544-551 (1982).
- ¹⁵ Koblentz-Mischke, O. J., Volkovinsky, V. V., Kabanova, J. G. Plankton primary production of the world ocean. *Scientific Exploration of the South Pacific* (ed Wooster, W.) 183–192 (National Academies Press, 1970).
- ¹⁶ Luz, B. & Barkan, E. Assessment of oceanic productivity with the triple-isotope composition of dissolved oxygen. *Science* **288**, 2028-2031 (2000).
- ¹⁷ Juranek, L. W. & Quay, P. D. Using triple isotopes of dissolved oxygen to evaluate global marine productivity. *Annu. Rev. Mar. Sci.* **5**, 503–24 (2013).
- ¹⁸ Carr, M. E. et al. A comparison of global estimates of marine primary production from ocean color. *Deep-Sea Res. II* **53**, 741–770 (2006).

² Falkowski, P. G., Laws, E. A., Barber, R. T., & Murray, J. W. Phytoplankton and their role in primary, new, and export production. In: *Ocean Biogeochemistry* (ed Fasham M. J. R.) 99-121 (Springer, New York, 2003).

¹⁹ Lee, Z., Marra, J., Perry, M. J. & Kahru M. Estimating oceanic primary productivity from ocean color remote sensing: A strategic assessment. *J. Mar. Syst.* **149**, 50–59, (2015).

- ²⁰ Antoine, D., André, J.-M. & Morel, A. Oceanic primary production 2. Estimation at global scale from satellite (coastal zone color scanner) chlorophyll. *Glob. Biogeochem. Cycles* **10**, 57–69 (1996).
- ²¹ Behrenfeld M. J., & Falkowski, P. G. Photosynthetic rates derived from satellite-based chlorophyll concentration. *Limnol. Oceanogr.* **42**, 1–20 (1997).
- ²² Buitenhuis, E. T., Hashioka, T. & Quéré, C. L. Combined constraints on global ocean primary production using observations and models. *Glob. Biogeochem. Cycles* **27**, 847–858 (2013).
- ²³ Gregg, W. W. & Rousseaux, C. S. Global ocean primary production trends in the modern ocean color satellite record (1998–2015). *Environ. Res. Lett.* **14**, 124011 (2019).
- ²⁴ Westberry, T. K., Behrenfeld, M. J., Siegel, D. A. & Boss, E. Carbon-based primary productivity modeling with vertically resolved photoacclimation. *Glob. Biogeochem. Cycles* **22**, GB2024, (2008).
- ²⁵ Saba, V. S., et al. The challenges of modeling depth-integrated marine primary productivity over multiple decades: A case study at BATS and HOT. *Glob. Biogeochem. Cycles* **24**, GB3020 (2010).
- ²⁶ Behrenfeld, M. J. et al. Revaluating ocean warming impacts on global phytoplankton. *Nat. Clim. Change* **6**, 323–330 (2016).
- ²⁷ Johnson, K. S. Simultaneous measurements of nitrate, oxygen, and carbon dioxide on oceanographic moorings: Observing the Redfield ratio in real time. *Limnol. Oceanogr.* **55**, 615–627 (2010).
- ²⁸ Nicholson, D. P., Wilson, S. T., Doney, S. C. & Karl, D. M. Quantifying subtropical North Pacific gyre mixed layer primary productivity from Seaglider observations of diel oxygen cycles. *Geophys. Res. Lett.*, **42**, 4032–4039 (2015).
- ²⁹ Barone, B., Nicholson, D., Ferrón, S., Firing, E. & Karl, D. The estimation of gross oxygen production and community respiration from autonomous time-series measurements in the oligotrophic ocean, *Limnol. Oceanogr.-Meth.* **17**, 650–664 (2019).
- ³⁰ Henderikx Freitas, F., White, A. E., & Quay, P. D. Diel measurements of oxygen and carbon based ocean metabolism across a trophic gradient in the North Pacific. *Global Biogeochem. Cycles*, **34**, e2019GB006518 (2020).
- ³¹ Gordon, C., Fennel, K., Richards, C., Shay, L. K., & Brewster, J. K. Can ocean community production and respiration be determined by measuring high-frequency oxygen profiles from autonomous floats? *Biogeosciences* **17**, 4119–4134, (2020).
- ³² Claustre, H., Johnson, K. S. & Takeshita, Y. Observing the global ocean with Biogeochemical-Argo. *Annu. Rev. Mar. Sci.* **12**, 23–48 (2020).
- ³³ Gille, S. T. Diurnal variability of upper ocean temperatures from microwave satellite measurements and Argo profiles. *J. Geophys. Res.* **117**, C11027 (2012).
- ³⁴ Juranek, L. W. & Quay, P. D. In vitro and in situ gross primary and net community production in the North Pacific subtropical gyre using labeled and natural abundance isotopes of dissolved O2. *Glob. Biogeochem. Cycles* **19**, GB3009 (2005).

³⁵ Quay, P. D., Peacock, C., Bjorkman, K. & Karl, D. M. Measuring primary production rates in the ocean: enigmatic results between incubation and non-incubation methods at Station ALOHA. *Glob. Biogeochem. Cycles* **24**, GB3014 (2010).

³⁶ Ferrón, S., Barone, B., Church, M. J., White, A. E. & Karl, D. M. *Euphotic zone metabolism in the North Pacific subtropical gyre based on oxygen dynamics. Global Biogeochem. Cycles* **35**, e2020GB00674 (2021).

- ³⁷ Luz, B. & Barkan, E. Assessment of oceanic productivity with the triple-isotope composition of dissolved oxygen. *Science* **288**, 2028-2031 (2000).
- ³⁸ Church, M. J., Lomas, M. W. & Muller-Karger, F. Sea change: Charting the course for biogeochemical time-series research in a new millennium. *Deep Sea Res. II* **93**, 2-15 (2013).
- ³⁹ Fawcett, S. E., Johnson, K. S., Riser, S. C., Van Oostende, N. & Sigman, D. M. Low-nutrient organic matter in the Sargasso Sea thermocline: a hypothesis for its role, identity, and carbon cycle implications. *Mar Chem.* **20**, 108–23 (2018).
- ⁴⁰ Huang, Y., Nicholson, D., Huang, B. & Cassar, N. Global estimates of marine gross primary production based on machine-learning upscaling of field observations. *Glob. Biogeochem. Cycles* GB006718 (2021).
- ⁴¹ Silsbe, G. M., Behrenfeld, M. J., Halsey, K. H., Milligan, A. J. & Westberry, T. K. The CAFE model: A net production model for global ocean phytoplankton. *Glob. Biogeochem. Cycles* **30**, 1756–1777 (2016).
- ⁴² Johnson, K. S. & H. Claustre (eds.) *The Scientific Rationale, Design and Implementation Plan for a Biogeochemical-Argo Float Array* (2016) https://doi.org/10.13155/46601.
- ⁴³ Kahru, M. Ocean productivity from space: Commentary. *Glob. Biogeochem. Cycles* **31**, 214-216 (2017).

Table 1. Gross Oxygen Production rates from 60°N to 60°S in water deeper than 2000 m. Annual GOP rates were calculated using all data in each latitude band. Volumetric GOP rates in column 4 are for the upper 20 m. GOP integrals in column 5 are to the 1% light level. VGPM, CBPM, and CAFE NPP values were calculated for years 2010 to 2019 using monthly values downloaded from the Oregon State University Ocean Productivity site (see Methods). Satellite rates were masked for depth using the ETOPO5 topography. Errors are 1 Standard Error.

Endis are 1 standard Entiti.									
Latitu	Area	Dept	GOP	GOP	GOP	Float	VGPM	CBPM	CAFE
de	10 ¹³	h 1%	mmol	mmol	Pmol O ₂	NPP	NPP	NPP	NPP
±5°	m ²	light	$O_2 m^{-3}$	$O_2 m^{-2}$	y ⁻¹	Pg C	Pg C	Pg C	Pg C
			d ⁻¹	d ⁻¹		y ⁻¹	y ⁻¹	y ⁻¹	y ⁻¹
55	1.09	39	3.5±1.3	77±26	0.31	1.4			
45	1.50	41	2.1±1.3	58±31	0.32	1.4	2.8	2.0	2.3
35	2.08	54	2.1±0.5	92±16	0.70	3.1	2.9	2.5	2.8
25	2.51	89	1.2±0.3	53±11	0.49	2.2	2.2	3.6	3.5
15	3.16	58	2.0±0.7	33±18	0.38	1.7	3.1	5.7	5.4
5	3.42	59	3.8±1.1	205±82	2.56	11.4	3.5	7.3	6.9
-5	3.38	64		205*	2.53*	11.2	4.0	7.7	7.2
-15	3.35	85		33*	0.40*	1.8	3.2	6.1	6.1
-25	3.10	91	0.8±0.3	30±10	0.34	1.5	2.7	4.4	4.3
-35	3.23	60	1.7±0.5	87±14	1.02	4.6	4.4	3.9	4.6
-45	3.04	62	2.9±0.4	121±10	1.34	6.0	4.2	3.0	4.5
-55	2.53	71	0.4±0.5	4±10	0.04	0.3	_	_	
Sum					10.4±1.6	46±7†	33	46	48

^{*}GOP values were estimated from corresponding rates in Northern Hemisphere due to a low number of float profiles.

^{†45} Pg C y⁻¹ without 55°N and 55°S bands.

Figure 1 Profile locations where primary production has been determined. a) Red dots are ¹⁴C profiles from the Oregon State University Ocean Productivity database, which includes profiles used to optimize the primary productivity model embedded in many satellite products^{21, 24}. Blue dots are the ¹⁴C profiles used, in addition to the OSU database, to optimize a GCM model of ocean productivity²². b) Float profile locations for floats with adjusted oxygen data and appropriate cycle timing. Green squares are the boundaries for float profiles used to determine GOP near HOT and BATS. Stations dots in both plots are the same size.

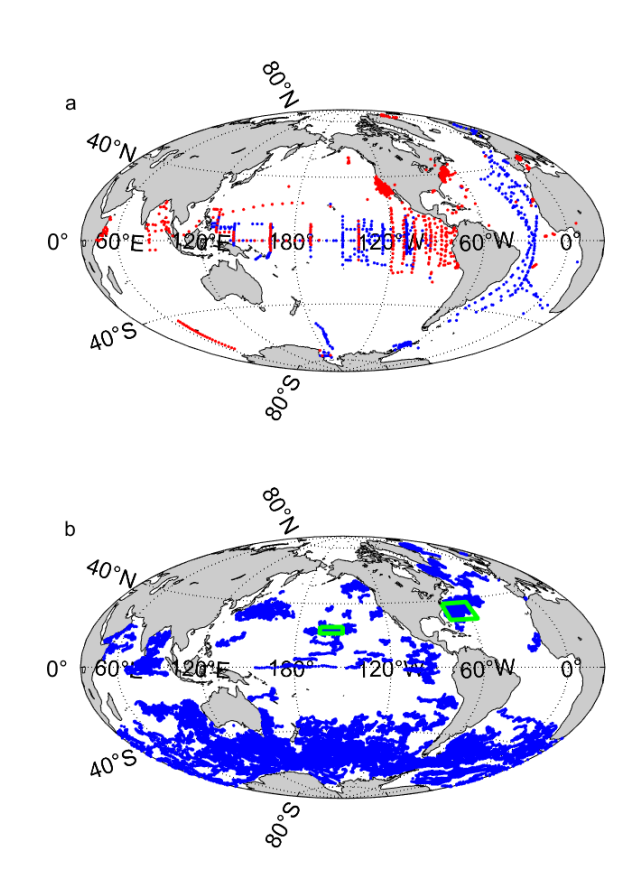


Figure 2 Northern hemisphere (60°N to 10°N) oxygen and GOP values. a) Mean oxygen anomaly in the upper 20 m from each profile with acceptable cycle timing (N=14,294) versus local hour of the day. Data from all days of year from 2010 through 2020 are included. b) Mean oxygen anomaly in each hourly interval and the least squares fit of Equation 2 to the data shown in a) with GOP = 2.2 ± 0.3 (1 Std Error) mmol O_2 m⁻³ d⁻¹. c) GOP determined each 2 months in the upper 20 m versus Day of Year. d) Depth profile of GOP rates for all days of the year. Error bars are one standard error.

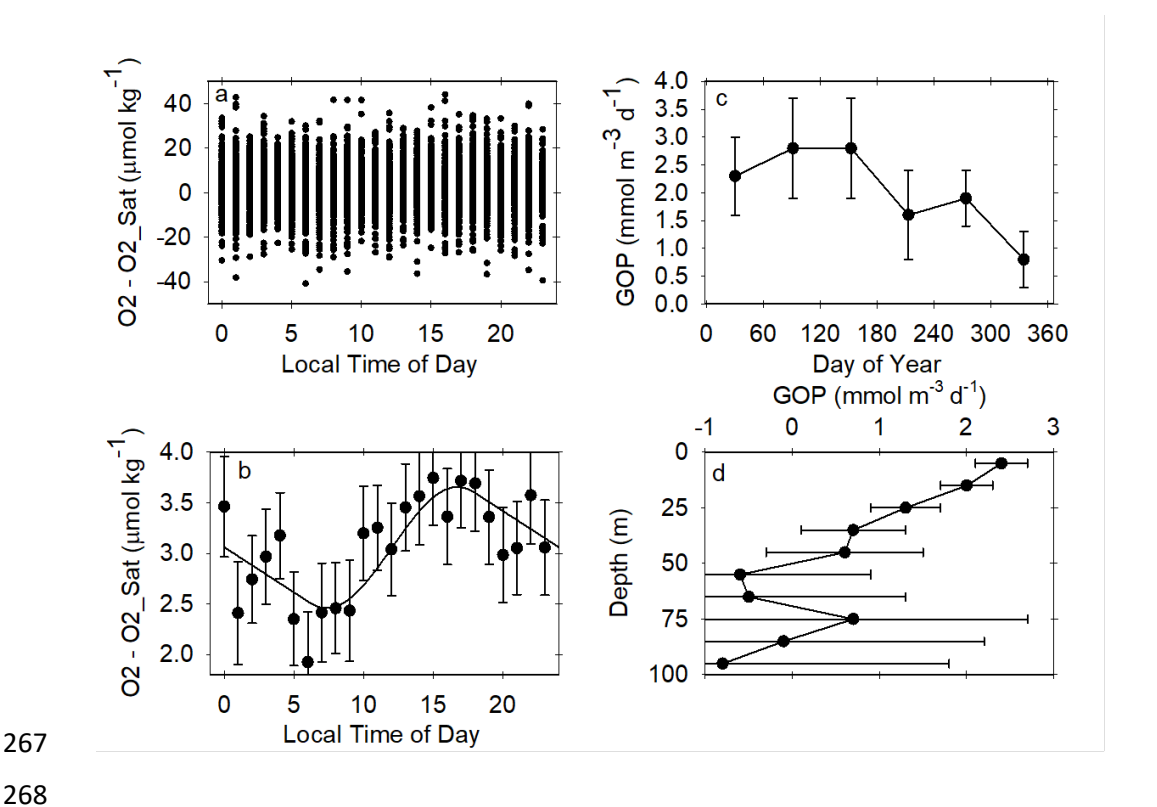
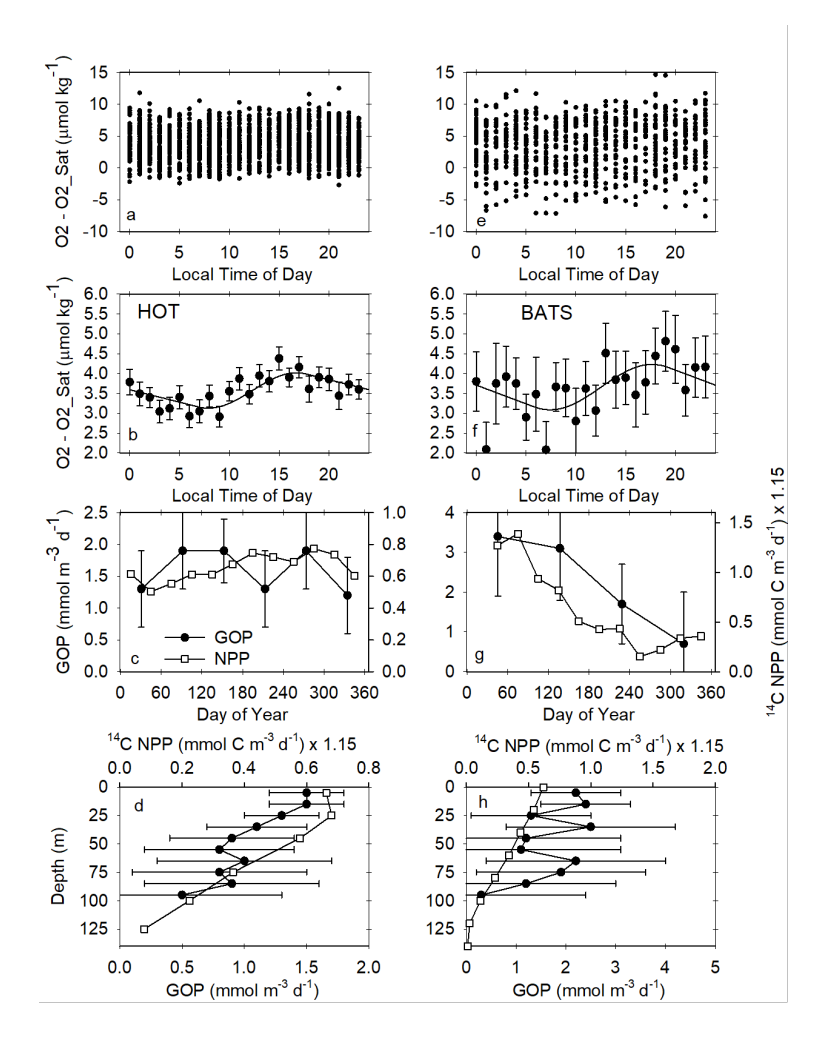


Figure 3. Oxygen anomalies and GOP from floats near the HOT and BATS time series stations. a) Oxygen anomaly from 2010 through 2020 in the upper 20 m near HOT versus hour of the day (Local Time). Data were collected and include all days of the year. b) Hourly mean oxygen anomaly values for samples near HOT and the least squares fit of Equation 2 to the data shown in a). c) GOP rates in the upper 20 m calculated at 2 month intervals using data shown in a) and the monthly mean NPP values observed at the HOT station ALOHA from 2010 to 2019. d) Vertical profile of GOP and the annual mean NPP rates at standard depths observed at the HOT station ALOHA. Panels e-f are the same for a region surrounding BATS. ¹⁴C primary productivity data are from the BATS station for 2010 to 2016. Error bars are 1 standard error.



Methods and Data

The Sprof profile files⁴⁴ from all Argo floats with oxygen sensors (N=1276) were downloaded from the Argo Global Data Assembly Center in December 2020. Only oxygen profiles with data that had been adjusted to correct for initial sensor calibration errors^{45, 46, 47} and with a quality flag equivalent to good were used. The data were further quality controlled to eliminate any floats with apparent errors in the adjusted data by plotting the adjusted oxygen percent saturation in the upper 10 m vs time. The adjusted data from 9 floats (Extended Data Table S1) had percent saturation values that appeared to be oceanographically inconsistent so they were removed from the data set. The BGC-Argo adjusted oxygen data have been corrected at the Argo Data Assembly Centers using two method. Floats that made air oxygen observations^{46, 48, 47} were corrected with an accuracy better than 1% of surface oxygen saturation concentration. Other floats, which did not make air oxygen measurements, were corrected using methods outlined in Takeshita et al.⁴⁵ with an accuracy near 3% of surface oxygen saturation concentration. All data was treated equivalently, without regard to the recalibration method, and no additional corrections to the adjusted oxygen concentrations were made. Extended Data Figure S1 shows all data in the upper 10 m that passed the additional quality control.

The analysis used here requires that each float has sampled all hours of the day at a relatively constant proportion so that any biases in sensor calibration are distributed equally into all hours of the day. Many floats make their profiles at non-integer intervals (approximately 5.2 or approximately 10.2 days) so that each subsequent profile occurs at a different hour of the day and nearly all hours are sampled over the lifetime of the float due to variability in timing. Any biases in the oxygen calibration of these floats would be present in all of the hourly samples. These biases would then appear as a constant offset in the diel cycle, but they would not alter the shape or the amplitude of the diel cycle. Other floats sample at one or a few fixed times of the day, often at local noon. Inclusion of the data from such floats in the analysis would introduce significant biases in both the shape and amplitude of the diel cycle because any oxygen calibration biases would appear in only a few of the hourly samples. Floats that sampled at only a few hours of the day were, therefore, removed from the analysis. Unfortunately, this latter class of floats constitutes the majority of the BGC-Argo array and their elimination reduced the number of available profiles by about two thirds.

Floats that did not sample all hours evenly were identified by computing the expected number of samples in each hour (local time) as the total number of profiles divided by 24. If the maximum number of profiles in any of the hourly bins exceeded the expected number by more than a factor of 3, that float was removed from the analysis. Individual data point that exceeded six times the standard deviation of all oxygen anomaly values used in a particular analysis were also removed to avoid influence from large outliers.

 The local time of day for each profile from floats with the required profiling timing was then computed. All of the oxygen anomaly data on individual profiles in each depth interval that was analyzed were averaged to a single value. This was done to avoid different weightings for the

profiles from floats that sample at different vertical resolutions. A pseudo-daily cycle was then created from the mean oxygen anomaly data from each profile at the local hour of day for a given region, desired depth range, and for the desired portion of the year. We have not corrected the data for the effects of gas exchange as the merged data set does not represent a continuous time series. In any case, the gas exchange corrections over a single pseudo-day represented by the data would be small, typically less than 10% given an oxygen residence time in the mixed layer near 2 weeks¹⁶.

The code developed by Barone et al.²⁹ was used to analyze the pseudo-daily cycles. This code was intended to allow the determination of both GOP and CR from a time series of oxygen data. However, the difference between GOP and CR, equivalent to Net Community Production, is small and typically about 10 to 20% of the GOP and CR values^{2, 28}. A single, pseudo-daily cycle of oxygen anomaly is not capable of resolving the difference in GOP and CR over one day, which will be at most a few tenths of 1 μ mol kg⁻¹. Further, as noted by Barone et al.²⁹, the GOP and CR values are highly correlated. With only a single daily estimate of the oxygen diel cycle, the best fits to the data may be reached with large, compensating errors in the GOP and CR. To control for this, we have assumed that GOP and CR are equal over a daily cycle. In the original method developed by Barone et al.²⁹, GOP and CR are determined by fitting basis functions to the oxygen data:

$$O2_Anom(t) = const. + GOP x f(t, E) - CR x t$$
 (1)

where f(t, E) is a basis function that describes the variability of GOP with local time (t) and light intensity (E) over a daily cycle. CR is presumed to be a constant rate and its basis function is time. Assuming GOP and CR are equal, we have simplified Equation 1 to:

$$O2_Anom(t) = const. + GOP x (f(t, E) - t)$$
 (2)

GOP was determined by fitting Equation 2 to all of the data in a pseudo-daily cycle. f(t, E) was determined using the Sinusoidal option described in Barone et al.²⁹, which assumes that GOP is directly proportional to the amount of available sunlight. The daily irradiance cycle was calculated at the mid-point of the time interval for sub-annual time periods. For annual cycles, the irradiance cycle was calculated at the median latitude of the data and for day 90 of the year. Experimentation with subsetting the datasets in time versus calculation with a single annual cycle shows that the single annual cycle introduces small (order of 10%) errors. We have used this protocol because some latitude bands in the final global analysis do not have enough data for subsetting.

 In the Figures 2 and 3, we highlight the quality of the GOP determinations by showing hourly averages of oxygen anomaly with the fit to Equation 2. We stress, however, that all of the data from each profile in a region at the selected depth interval and time period were used to create the fit, not the hourly averages.

Several possible, systematic errors are present in the GOP values determined in each region. Diel heating can bias GOP values high. Warmer daytime temperatures reduce the computed oxygen solubility, which increases the oxygen anomaly and apparent GOP. The largest diel temperature amplitudes occur during summer at the equator and are around 0.1°C³³. Computation of the daily temperature cycle with the floats studied here requires contemporaneous analysis of satellite data and large numbers of floats, which is beyond the scope of this study. To assess the magnitude of this error, we have imposed a 0.1°C diel temperature cycle on the hourly mean data from the 5°N band in Table 1. This shifts the GOP rates computed with the hourly mean anomalies, rather than all of the individual profile anomaly values as is done in Table 1, from 4.0±1.1 mmol O₂ m⁻³ d⁻¹ to 3.6±1.3 mmol O₂ m⁻³ d⁻¹. This is the likely maximum error that results from neglecting diel heating since the temperature amplitude is largest at the equator. Neglecting diel heating has increased GOP by order of +10%.

The bias high due to neglect of diel heating is countered by two processes that tend to lower GOP. First, outgassing of O_2 over the course of a pseudo-day will reduce the amplitude of the diel cycle and lower GOP. Given typical piston velocities for gas exchange, this may reduce GOP by 10%. Correcting for gas exchange in the 5°N band with a large piston velocity of 10 m d⁻¹, typical for a wind velocity of 10 m s⁻¹ while global mean wind speed over the ocean is 7 m s⁻¹ (Ref. 49), and a shallow mixed layer of 30 m would increase GOP to 4.3 ± 1.3 mmol O_2 m⁻³ d⁻¹. The small effect of gas exchange on determination of GOP from diel cycles in the open ocean is consistent with the prior work²⁹. Gas exchange about counters the neglect of heating. Second, t the assumption that GOP equals CR will also bias the computed GOP value low in an autotrophic ocean⁵⁰. Global net community production, equal to GOP – CR, is typically less than 5 mol C m⁻² y⁻¹ in the open ocean⁵¹, which is equivalent to a bias of 0.3 mmol C m⁻² d⁻¹. This is likely the maximum bias due to this assumption in the open ocean.

The sum of all three biases will approach zero. As a result, these three processes have been assumed to have negligible effect on the GOP. The reasonable agreement of the observed GOP values near HOT and BATS, and the agreement with the global GOP estimate of Huang et al.⁴⁰ support this assumption.

Primary production rates are generally integrated vertically, typically to the 1% light level. To assess the depth of the 1% light level, we used chlorophyll fluorescence profiles observed with fluorometers on BGC-Argo floats in each of the domains analyzed. Adjusted chlorophyll values were processed following Argo protocols⁵². Daytime profiles were corrected for non-photochemical quenching and all chlorophyll values computed from the manufacturer's calibration were divided by a factor of 2 to correct for a global bias in the sensor calibration⁵³. Total chlorophyll was then corrected for sensor background signals with a modified version of the algorithm described in Briggs et al.⁵⁴ Each float and sampled year was corrected separately. The method was also tuned to accommodate the vertical resolution of chlorophyll measurements on many floats that is lower than the high-resolution profiles used by Briggs et al.⁵⁴. The approximate 0.5% light level for each latitude bin (the primary production zone, PPZ) was then determined as the depth where chlorophyll signals dropped to 10% of the maximum

above that depth⁵⁵. The 1% level was then calculated assuming an exponential decrease in 412 413 chlorophyll levels down to the PPZ. To confirm the calculations of light level, the euphotic zone 414 depth (1% light level) was also calculated using the equation reported in Morel⁵⁶ and the climatological surface chlorophyll concentration observed by the MODIS ocean colour satellite. 415 The float based 1% light level is highly correlated with the values derived from MODIS 416 chlorophyll for the 10° latitude bins, but the float based value is about 20% shallower. Float 417 values were also comparable to those reported in Buesseler et al. 55. We preferred the 1% light 418 levels calculated from the chlorophyll fluorescence profiles as GOP values often became 419 420 negative and not statistically significant at greater depths. The uncertainty in the integrated GOP profile was obtained as the square root of the sum of the squared standard errors of 421 integrated rates in 10 m vertical bins down to the 1% light level. Note that we have included 422 423 negative values of GOP in the integrals that were found above the 1% light level in most cases. 424 Small negative values result from random noise when GOP is near zero at depth and are 425 retained to avoid biasing the results. However, large negative values of GOP, at the base of the 426 euphotic zone in the 25°N and 15°N bands, were excluded as they resulted from large variability 427 in the oxygen anomaly caused by shallow oxygen minimum zones.

428 429

430

431

432

433 434

435 436

437

438

439 440

441

442 443

444 445 Annual mean values of NPP were computed for the years 2010 to 2019 with the VGPM²¹, CBPM²⁴, and CAFE⁴¹ NPP models. Monthly mean NPP data for each model were downloaded from the Oregon State University Ocean Productivity site (https://sites.science.oregonstate.edu/ocean.productivity/). The monthly means were summed for each year and then an annual mean for 2010 to 2019 was determined. To be directly comparable to float observations, regions shallower than 2000 m were masked out of the means using the ETOP05 data set⁵⁷. The data for many months poleward of 50° are missing due to persistent cloud coverage. Using data in this region requires extensive gap-filling and we have not computed means poleward of 50°. The gap-filled, global means reported for the VGPM, CBPM, and CAFE models (44, 52, and 52 Pg C y⁻¹, respectively)^{21, 24, 41} were used instead. The summed GOP and NPP values in Table 1 for the latitude range 50° N to 50°S were then extrapolated to a global extent by multiplying by 1.18. The value of 1.18 is the mean ratio of the reported global total NPP for each satellite algorithm to the summed NPP values for the algorithms from 50° N to 50°S (Table 1). This factor corrects for areas at high latitudes that were not analyzed and for high productivity in coastal zones that was not sampled by profiling floats. These high productivity coastal zones were omitted from the satellite calculations by masking out regions shallower than 2000 m.

⁴⁴ Bittig, H., Wong, A., & Plant, J. *BGC-Argo Synthetic Profile File Processing and Format On Coriolis GDAC*, v1.21 (2021) https://dx.doi.org/10.13155/55637

⁴⁵ Takeshita, Y. *et al.* A climatology-based quality control procedure for profiling float oxygen data. *J. Geophys. Res. Oceans* **118**, 5640–5650 (2013).

⁴⁶ Johnson, K. S., Plant, J. N., Riser, S. C. & Gilbert, D. Air oxygen calibration of oxygen optodes on a profiling float array. *J. Atmos. Ocean. Technol.* **32**, 2160–2172 (2015).

⁴⁷ Bittig, H. C. et al. Oxygen optode sensors: principle, characterization, calibration, and application in the ocean. *Front. Mar. Sci.* **4**, 429 (2018).

⁴⁸ Johnson, K. S. et al. Biogeochemical sensor performance in the SOCCOM profiling float array. *J. Geophys. Res.* **122**, 6416–6436 (2017).

⁴⁹ Wanninkhof, R. Relationship between wind speed and gas exchange over the ocean revisited. *Limnol. Oceanogr. Methods* **12**, 351-362 (2014).

⁵⁰ Riser, S. C. & Johnson, K. S. Net production of oxygen in the subtropical ocean. *Nature* **451**, 323–325 (2008).

⁵¹ Emerson, S. Annual net community production and the biological carbon flux in the ocean. *Global Biogeochem. Cycles*, **28**, 14-28, doi:10.1002/2013GB004680.

⁵² Schmechtig, C., Poteau, A., Claustre, H., D'Ortenzio, F. & Boss, E. *Processing Bio-Argo Chlorophyll-a Concentration at the DAC Level*. http://doi.org/10.13155/39468 (Ifremer, 2015).

⁵³ Roesler, C., Uitz, J., Claustre, H., Boss, E., Xing, X., Organelli, E., Briggs, N., Bricaud, A., Schmechtig, C., Poteau, A., D'Ortenzio, F., Ras, J., Drapeau, S., Haëntjens, N. and Barbieux, M. Recommendations for obtaining unbiased chlorophyll estimates from in situ chlorophyll fluorometers: A global analysis of WET Labs ECO sensors. *Limnol. Oceanogr. Methods* **15**: 572–585 (2017).

⁵⁴ Briggs, N., Dall'Olmo, G. & Claustre, H. Major role of particle fragmentation in regulating biological sequestration of CO2 by the oceans. *Science* **367**, 791-793 (2020).

⁵⁵ Buesseler, K.O., Boyd, P.W., Black, E.E. & Siegel, D.A. Metrics that matter for assessing the ocean biological carbon pump. *Proc. Natl. Acad. Sci.* **117**, 9679-9687 (2020).

⁵⁶ Morel, A. et al. Examining the consistency of products derived from various ocean color sensors in open ocean (Case 1) waters in the perspective of a multi-sensor approach. *Remote Sens. Environ.* **111**, 69–88 (2007).

⁵⁷ National Geophysical Data Center. *ETOPO5: Data Announcement 88-MGG-02, Digital Relief of the Surface of the Earth* (NOAA, 1988); https://doi.org/10.7289/V5C8276M

 Acknowledgements This work was supported by the Global Ocean Biogeochemical Array project (NSF OCE-1946578; publication #1), the Southern Ocean Carbon and Climate Observations and Modeling project (NSF PLR-1425989 and OPP-1936222), and the David and Lucile Packard Foundation. Profiling floats in the Equatorial Pacific were supported by NOAA under grant NA16OAR4310161 to the University of Washington. We thank Jacki Long for assistance with the satellite data, and Tanya Maurer and Josh Plant for processing data and assistance with coding. Steve Riser and Dana Swift prepared many of the profiling floats whose data were used in this analysis. We thank the Hawaii-Ocean Time-series and Bermuda Atlantic Time-series Station programs for making their data easily accessible. The float data were collected and made freely available by the International Argo Program and the national programs that contribute to it (https://argo.ucsd.edu, https://www.ocean-ops.org). The Argo Program is part of the Global Ocean Observing System. The manuscript was greatly improved, and several misconceptions were identified, by the anonymous reviews. We thank them for their efforts.

 Author Contributions K. S. J. conceived the study, performed final data analysis, and drafted the initial manuscript. M. B. B. developed analytical methods and performed exploratory data analyses and contributed to the interpretation of results and writing of the manuscript.

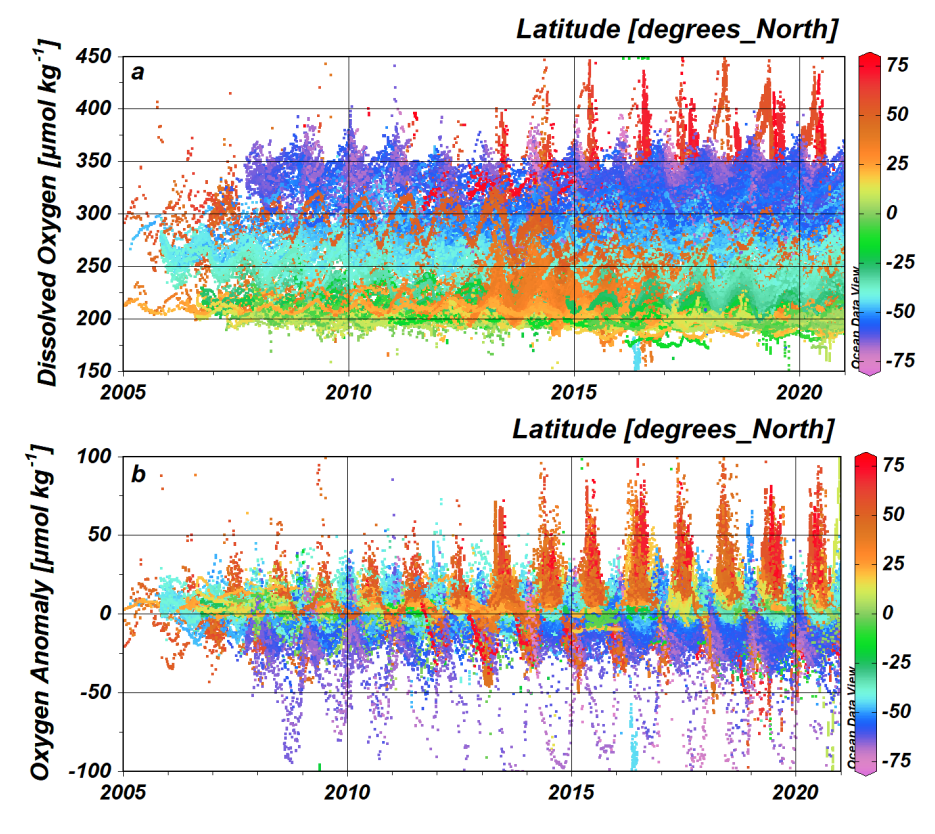
Competing Interest Declaration The authors declare that they have no competing financial interests.

Corresponding Author Correspondence and requests for materials should be addressed to K.S.J. (johnson@mbari.org).

Extended Data Table S1. WMO numbers of floats with inconsistent oxygen concentrations and not used in this analysis.

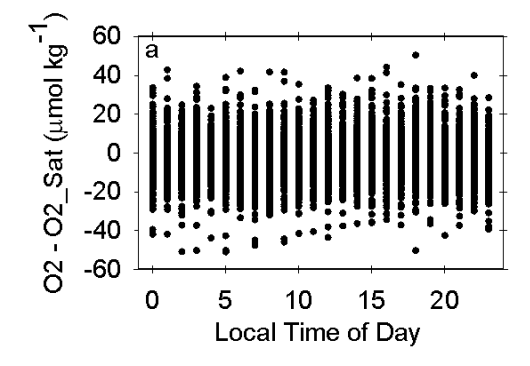
Floats
removed
2902087
2902123
4901137
4901140
4901141
4901784
5900420
5901178
7900559

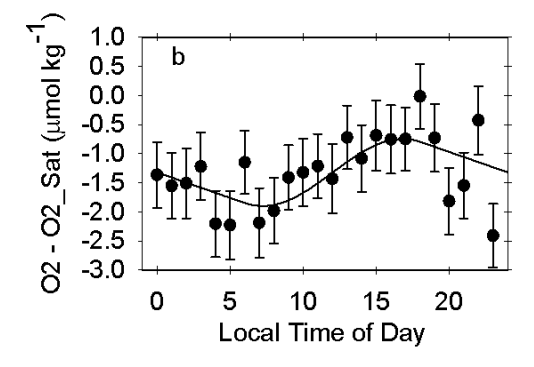
Extended Data Figure S1. Profiling float oxygen data. a) Dissolved oxygen and b) Oxygen Anomaly = Oxygen – Oxygen Saturation in the upper 10 m for all adjusted oxygen data with quality flag = 1 (good data) in the Argo Global Data Assembly Center, except for 9 floats listed in Extended Data Table S1.



Extended Data Figure S2. Global (60°N to 60°S) oxygen and GOP values for the years 2016 through 2020. a) Mean oxygen anomaly in the upper 20 m from each profile with acceptable cycle timing versus local hour of the day. b) Mean oxygen anomaly in each hourly interval and the least squares fit of Equation 2 to the data shown in a) with GOP = 2.1 ± 0.4 (1 Std Error) mmol O_2 m⁻³ d⁻¹.







Extended Data Figure S3. Annual mean NPP rates from 2010 through 2020 in each 10° latitude band from 50°N to 50°S. a) Float and satellite NPP rates versus latitude. b) Satellite NPP rates in each 10° latitude band for each model versus float NPP rates. Satellite NPP models include VGPM²¹, CBPM²⁴, and CAFE⁴¹. All values from Table 1.

